Joint Resource Allocation and UAV Scheduling With Ground Radio Station Sleeping

AKHILESWAR CHOWDARY[1], **(Graduate Student Member, IEEE),**
YOGHITHA RAMAMOORTHI[2], **(Member, IEEE), ABHINAV KUMAR**[1], **(Senior Member, IEEE),**
AND LINGA REDDY CENKERAMADDI[3], **(Senior Member, IEEE)**
[1]Department of Electrical Engineering, Indian Institute of Technology Hyderabad, Sangareddy, Telangana 502285, India
[2]NTT Access Network Service Systems Laboratories, Yokosuka 239-0847, Japan
[3]Department of Information and Communication Technology, University of Agder, 4879 Grimstad, Norway

Corresponding author: Linga Reddy Cenkeramaddi (linga.cenkeramaddi@uia.no)

ABSTRACT Applications of Unmanned aerial vehicles (UAVs) have advanced rapidly in recent years. The UAVs are used for a variety of applications, including surveillance, disaster management, precision agriculture, weather forecasting, etc. In near future, the growing number of UAV applications would necessitate densification of UAV infrastructure (ground radio station (GRS) and ground control station (GCS)) at the expense of increased energy consumption for UAV communications. Maximizing the energy efficiency of this UAV infrastructure is important. Motivated by this, we propose joint resource allocation and UAV scheduling with GRS sleeping (GRSS). Further, we propose the use of coordinated multi-point (CoMP) with joint transmission (JT) and non-orthogonal multiple access (NOMA) along with GRSS to increase the coverage and data rates, respectively. Through exhaustive simulation results, we show that the proposed CoMP along with GRSS results in up to 10% higher energy savings and 24% increase in coverage. Further, NOMA along with GRSS results in up to 9% enhancement in throughput of the system.

INDEX TERMS Coordinated multi-point (CoMP), ground control station (GCS), ground radio station sleeping (GRSS), non-orthogonal multiple access (NOMA), unmanned aerial vehicle (UAV).

I. INTRODUCTION

Now-a-days, Drones are being used in a wide variety of applications like surveillance, disaster management, communication, weather forecast, wildlife monitoring, aerial photography, shipping and delivery, 3D mapping [1]. With an increasing number of applications, unmanned aerial vehicles (UAVs), also known as Drones, will soon be densely populating the low-altitude air space. These UAV deployments are expected to provide highly reliable communication in various scenarios [2]. To ensure autonomous UAV operations, one of the key requirements is reliable communication links with ground infrastructure. Communication with UAV is broadly divided into two components [3]. One of them is the Control and Non-payload communication (CNPC) link and the other is the Payload data link. The CNPC link plays a key role in

The associate editor coordinating the review of this manuscript and approving it for publication was Ghufran Ahmed.

delivering telecommand and telemetry information such as flight control, status monitoring, location, etc. The Payload data link delivers the data to both the parties, i.e., from the GRS to the UAV and vice versa. A reliable CNPC link is essential to ensure the secure integration of UAVs into national air space (NAS). Hence, this paper deals with the CNPC links.

In recent years, a considerable amount of work has been done in the area of CNPC channel modelling. In [5]–[7], the authors have published a series of works related to CNPC channel modelling for different environments. In [5], the channel model has been developed for over-water settings. In [6] and [7], the authors have analysed channel in hilly and mountainous settings, and suburban and near-urban environments, respectively, in the frequency bands allotted by World radio conference-12 (WRC-12) [3] for CNPC operation. In [8], the authors have presented UWB channel modelling for air-to-ground propagation channels.
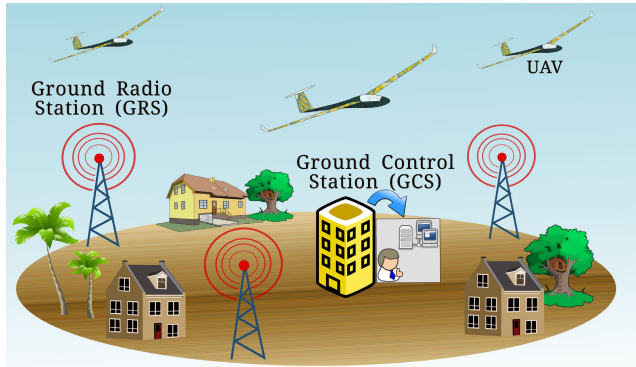
FIGURE 1. System model.

In [9], UAV air-to-ground channel model has been developed for mmWave systems. In [10], [11], the authors have analysed the Doppler effect on the air-to-ground channel and the methods to mitigate the same. Several works like [12]–[19] have considered UAV deployment as the aerial base station and considered coverage analysis, optimal altitude deployment, user association etc. However, resource allocation and energy efficiency for UAV communications have not been considered.

The secure integration of UAVs into NAS is not possible without analysing the GRS network. The GRS is an important part of the network which aids in establishing communication with the UAV and allocates resources to the UAVs accordingly. GRS is the most energy consuming unit in the UAV communications like Base station (BS) in cellular network. Base station sleeping (BSS) is a known technique for energy efficient operation in cellular network [20]. In general, every network is designed for a nominal number of users (here UAVs). Like any other network [20], we expect in a UAV network also the UAV density would vary with time and falls below certain threshold at multiple instants. In such scenarios, we investigate whether some GRSs can be moved into sleep mode to conserve energy while still maintaining QoS. Motivated by it, this is the first work that explores GRSS for energy efficient UAV communication network.

Coverage and throughput issues with BSS have been addressed in [20] and [21] using CoMP with JT and NOMA, respectively. Motivated by this, we consider CoMP with JT and NOMA with GRSS in this paper. We use CoMP with JT interchangeably with CoMP throughout the text. The trade-off between energy, coverage, throughput for GRSS, joint GRSS and CoMP, and joint GRSS and NOMA considering the mobility of the UAV has not been much discussed in the literature. This is the motivation of our work. The major contributions of this paper are as follows:

- We formulate the GRS sleeping optimization problem which ensures quality of service (QoS) to each UAV when GRS is in sleep mode.
- We design a dynamic GRS sleeping algorithm that ensures QoS to each UAV when GRS is in sleep mode.

- We propose a joint GRSS and CoMP algorithm to compensate for the coverage loss due to GRSS.
- We propose a joint GRSS and NOMA algorithm to compensate for the throughput drop due to GRSS.
- We present extensive simulation results of the proposed algorithms and provide a comparative study of these results with the benchmark system, benchmark with CoMP, and benchmark with NOMA.

The rest of the paper is organized as follows. Section II describes the System model. Section III includes the problem formulation. Section IV and Section V, respectively, give the details of CoMP and NOMA considered in this paper. The proposed algorithms are presented in Section VI. Extensive numerical results are presented in Section VII. Section VIII gives the concluding remarks.

II. SYSTEM MODEL

We consider a randomly deployed homogeneous OFDMA based GRS network in which the set of GRSs and UAVs in the network are denoted using $\mathcal{G} = \{1, 2, 3, \ldots, G\}$ and $\mathcal{U} = \{1, 2, 3, \ldots, U\}$, respectively. We consider that the UAVs and GRSs are deployed randomly with density λ_u per km^2 and λ_g per km^2, respectively. In Fig. 1, we present the system model considered in this work [22]. In this paper, we focus on the downlink, however, similar results can also be obtained for uplink. Without loss of generality, here we assume that the GRSs are divided into clusters of size n. However, this framework can be extended to varying cluster sizes. We consider a clustering based on distance among the GRSs. Alternatively, any other clustering mechanism can also be considered. There are various other ways of clustering like K-means clustering [23] etc. Let $\mathcal{M} = \{1, 2, 3, \ldots, M\}$ denote the set of sub-channels available in the network. All important mathematical notations used in this paper are summarized in Table 1. Next, we discuss the spectrum allocation for UAV communication considered in this paper.

A. SPECTRUM ALLOCATION FOR UAV COMMUNICATIONS

Since CNPC carries telecommand and telemetry information, the International Civil Aviation Authority (ICAO) has decided to operate these links in secure bands designated by International Telecommunications Union (ITU). The designations [3] are as follows:

- Aeronautical mobile (route) service (AM(R)S) for terrestrial CNPC.
- Aeronautical mobile-satellite (route) service (AMS(R)S) for satellite CNPC for Beyond line of sight BLOS) CNPC.

The spectrum requirements for the Unmanned aircraft systems CNPC (UAS CNPC) are officially defined by the ITU radio-communications sector (ITU-R) considering the data requirements and UAV density estimated for the year 2030. The bandwidth allocation [3] is as follows:

- 34 MHz for the terrestrial-based LOS CNPC.
- 56 MHz for satellite-based BLOS CNPC.

TABLE 1. Mathematical notations.

$A_{a1/a2}$	GRS sleeping pattern in which $a1$ out of $a2$ are in sleep mode
$ES_{n-i/n}$	Percentage of Energy saved
$F_{u,g}$	Free space path loss term between UAV u and GRS g
$\mathcal{G}$	Set of GRS
$\mathcal{G}_k$	Set of GRS in cluster k
h_0	Altitude at which UAVs are deployed
$h_{u,g}^m$	channel gain between UAV u and GRS g on the subchannel m
$\mathcal{K}$	Set of Clusters
$\mathcal{M}$	Set of subchannels
P_g^m	Power allocated by GRS g to the UAV u on the subchannel m
$PL_{(u,g)}$	Pathloss between UAV u and GRS g
$P_{LOS(u,g)}$	Probability of Line of sight between UAV u and GRS g
$P_{NLOS(u,g)}$	Probability of Non line of sight between UAV u and GRS g
$r_{u,g}^m$	Link rate of UAV u with GRS g on the subchannel m
R_u	Data rate of UAV u
S	SINR threshold for minimum QoS
T_α	α-fair throughput over the set of UAVs
$\mathcal{U}$	Set of UAVs
$\mathcal{U}_k$	Set of UAVs in cluster k
$\mathbf{U}_\alpha$	Utility function for α-fair scheduler
$x_{u,g}^m$	Binary association of UAV u with GRS g on the subchannel m
α	Fairness parameter for a fair scheduler
$\beta_{u,g}$	Time fraction allocated to a UAV u by GRS g
$\gamma_{u,g}^m$	SINR received by a UAV u from a GRS g on a subchannel m
Γ	SINR vector of all UAVs at time instant t in cluster k
$\Gamma_{a1/a2}$	SINR vector of all UAVs at time instant t in cluster k for a GRS sleeping configuration $a1/a2$
$\hat{\Gamma}_{a1/a2}$	SINR vector of all UAVs at time instant t in cluster k for a GRS sleeping configuration $a1/a2$ when CoMP is considered
$\tilde{\Gamma}_{a1/a2}$	SINR vector of all UAVs at time instant t in cluster k for a GRS sleeping configuration $a1/a2$ when NOMA is considered
Δ	Area considered for deployment of GRSs and UAVs
δ	Step size of the time interval
ζ_b	Fraction of total power allocated to strong UAV in the bth NOMA pair
$\eta(\cdot)$	Spectral efficiency in $bits/symbol$
θ_k	CoMP cluster time fraction
λ_g	GRS Density per km^2
λ_u	UAV Density per km^2
μ_k^t	Throughput of the cluster k at time t
ν	Velocity of the UAV
ξ_a	Active mode power consumption by GRS
ξ_s	Sleeping mode power consumption by GRS
χ	SINR threshold for CoMP
τ_k	Rate threshold for a cluster k
Ψ	Rate vector k of all UAVs at time instant t in cluster k
$\Psi_{a1/a2}$	Rate vector of all UAVs at time instant t in cluster k for a GRS sleeping configuration $a1/a2$
$\hat{\Psi}_{a1/a2}$	Rate vector of all UAVs at time instant t in cluster k for a GRS sleeping configuration $a1/a2$ when CoMP is considered
$\tilde{\Psi}_{a1/a2}$	Rate vector of all UAVs at time instant t in cluster k for a GRS sleeping configuration $a1/a2$ when NOMA is considered

World radiocommunication conference in 2012 recommended a new spectrum for AM(R)S for UAS CNPC. The spectrum assigned is as follows [3]:

- 5030 MHz - 5091 MHz (C-band).
- 960 MHz - 1164 MHz (L-band).

In this paper, we consider L-band for numerical analysis. However, the algorithms which we propose further are equally valid for other bands. Next, we present the power allocation and UAV association considered in this work.

B. POWER ALLOCATION AND PHYSICAL CHANNEL MODEL

Let P_g denote the total power transmitted by a GRS. We consider the power allocated per subchannel m by the GRS g as follows.

$$P_g^m = \frac{P_g}{M}, \quad \forall m \in \mathcal{M}. \tag{1}$$

The signal-to-interference-plus-noise ratio (SINR) of a UAV u from a GRS g, denoted by $\gamma_{u,g}^m$, on a subchannel m is given as

$$\gamma_{u,g}^m = \frac{P_g^m h_{u,g}^m}{\sum_{\substack{\hat{g} \neq g \\ \hat{g} \in \mathcal{G}}} P_{\hat{g}}^m h_{u,\hat{g}}^m + \sigma^2}, \tag{2}$$

where, P_g^m is the power allocated to the subchannel m by the GRS g as in (1), $\sum_{\substack{\hat{g} \neq g \\ \hat{g} \in \mathcal{G}}}^m P_g^m h_{u,\hat{g}}^m$ is the interference on the subchannel m, and σ^2 is the noise power. $h_{u,g}^m$ denotes the channel gain between the UAV u and the GRS g and it is given as follows.

$$h_{u,g}^m = 10^{\left(\frac{-PL(u,g) + G_g(\phi) + G_u - \upsilon - \rho}{10}\right)}, \tag{3}$$

where, G_u is the antenna gain, υ is the penetration loss, ρ is the loss due to small scale fading as in [24], $G_g(\phi)$ is the directivity gain, and $PL(u, g)$ is the path loss for the distance d between u and g. The pathloss between UAV and GRS as in [7] is written as follows.

$$PL_{(u,g)} = F_{u,g} + 10n \log\left(\frac{d}{d_{min}}\right) + X,$$

where, n is the path loss exponent, d is the propagation distance, d_{min} is the minimum distance of a UAV from the GRS, and X is the shadowing variable. $F_{u,g}$ is the free space path loss term with center frequency f_c and is as follows [7].

$$F_{u,g} = 92.45 + 20 \log(f_c) + 20 \log(d_{min}).$$

We consider Line of sight (LOS) probability, P_{LOS} as in [22] and it is expressed as

$$P_{LOS(u,g)}(\theta_{d_0}) = \frac{1}{1 + C \exp(-B(\theta_{d_0} - C))}, \tag{4}$$

TABLE 2. Modulation and coding scheme.

SINR Threshold(dB)	-6.5	-4	-2.6	-1	1	3	6.6	10	11.4	11.8	13	13.8	15.6	16.8	17.6
Efficiency (bits/symbol)	0.15	0.23	0.38	0.60	0.88	1.18	1.48	1.91	2.41	2.73	3.32	3.9	4.52	5.12	5.55

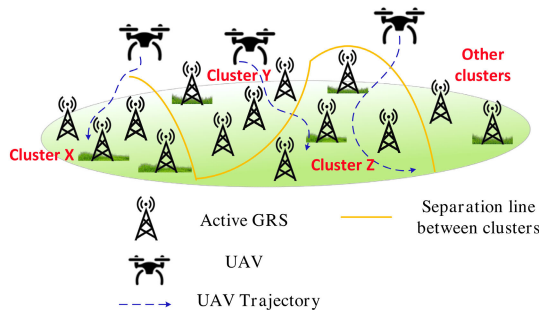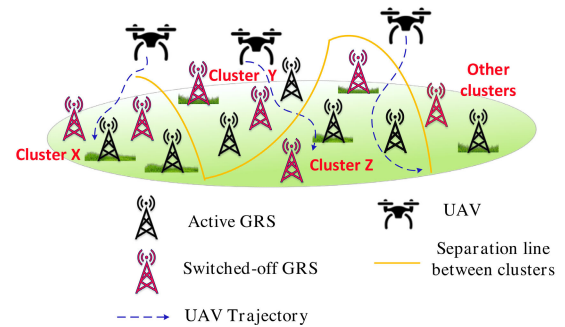**FIGURE 2. When all GRSs in the cluster are active.**

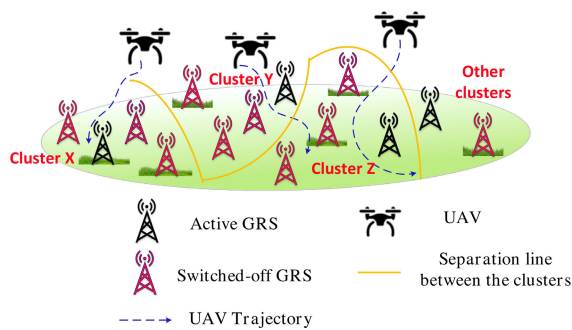**FIGURE 3. When 3 out of 4 GRSs in the cluster are in sleep mode.**

FIGURE 4. When 2 out 4 GRSs in the cluster are in sleep mode.
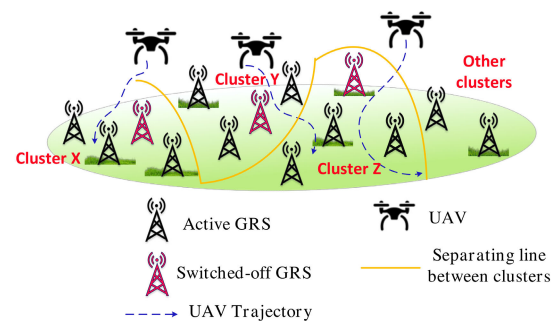

FIGURE 5. When 1 out of 4 GRSs in the cluster is in sleep mode.

where, θ_{d_0} is the elevation angle which is expressed as $\theta = tan^{-1}(h_0/d_0)$, h_0 is the altitude of UAV, and d_0 is the horizontal distance between UAV u and GRS g. B and C are environment-dependent constants. Similarly, the NLOS probability can be expressed from (4) as $P_{NLOS}(\theta_{d_0}) = 1 - P_{LOS}(\theta_{d_0})$. Next, we discuss the UAV association considered in this paper.

C. UAV ASSOCIATION

Given P_g^m as the power allocated by the GRS g to the UAV u on the subchannel m, we consider the UAV association with the GRS based on the maximum received power. Let $x_{u,g}^m$ denote the binary association of UAV u with GRS g on the subchannel m and is given as

$$x_{u,g}^m = \begin{cases} 1, & \text{if } g = \arg\max_g\{P_g^m h_{u,g}^m\}, \\ 0, & \text{otherwise, } \forall u \in U, \ \forall g \in G, \end{cases} \quad (5)$$

where, $h_{u,g}^m$ is the channel gain between UAV u and GRS g on the subchannel m as in (3). The binary variable $x_{u,g}^m$ is 1 when the UAV u associates with GRS g and is 0 otherwise. Next, we discuss link rate of the UAV considered in this paper.

D. RATE COMPUTATION

We consider adaptive modulation and coding scheme (MCS) which is summarized in Table 2 for mapping SINR to spectral efficiency as in [25]. Let, $\eta(\gamma_{u,g}^m)$ denote the spectral efficiency of a UAV u on a subchannel m in bits/symbol from GRS g. The link rate of UAV u from the GRS g with the spectral efficiency $\eta(\gamma_{u,g}^m)$ is

$$r_{u,g} = \frac{\eta(\gamma_{u,g}^m)SC_{OFDM}SY_{OFDM}}{T_{sc}}\text{M}, \quad (6)$$

where, SC_{OFDM}, SY_{OFDM}, and T_{sc} represent the number of subcarriers per channel, number of symbols used per subcarrier, and time duration of a subframe, respectively. M represents the number of subchannels.

We consider an α-fair time-based scheduler at each GRS which allocates all the M subchannels for a downlink UAV scheduling time fraction denoted by $\beta_{u,g}$ to a UAV u associated with it. We have considered the maximum received power based association of UAVs with the GRSs as in 5. Thus, for a UAV u, $\beta_{u,g}$ is non-zero for only one GRS g. The resultant downlink rate for any UAV u is given as

$$R_u = \sum_{g \in \mathcal{G}} \beta_{u,g} r_{u,g}. \quad (7)$$

Next, we present the UAV distribution considered in this work.

E. UAV DISTRIBUTION

We denote the area under consideration as Δ. The UAVs are assumed to be distributed randomly using PPP in the

considered area with an average UAV density of λ_u per km^2. The set of UAVs associated with GRS cluster k at time t is represented by $\mathcal{U}_k$ and the number of UAVs associated with this cluster be denoted by Ω. As already mentioned, CNPC links carry critical information pertaining to UAV navigation. Compromising with QoS in such scenarios can be disastrous. So, GCS should keep track of the SINR of UAVs and update the sleeping patterns accordingly. The GCS would update the sleeping patterns periodically using the recently updated SINR estimates. Next, we present the GRS distribution and sleeping patterns considered in this work.

F. GRS DISTRIBUTION AND SLEEPING PATTERNS
The GRSs are deployed randomly using Poisson point process (PPP) in the area Δ with an average density of λ_g per km^2. The set of GRSs in a cluster k is represented by $\mathcal{G}_k$. As shown in Fig. 1, a GCS which consists of an air traffic controller (ATC) and other necessary equipment would control all the GRSs currently being operated in its jurisdiction. However, to focus on GRS sleeping we do not represent GCS in the figures after Fig.1 in this paper. Whenever a UAV enters into the coverage area of a cluster, the trajectory information of that particular UAV will be shared with the GCS handling that cluster. With the trajectory information and log files of all UAVs currently operating in that cluster, a dynamic energy-saving procedure can be initiated by the GCS. The GRS can estimate the SINR and rate of any UAV in its coverage. The GRS shares this information with the GCS which can then decide based on the UAV load in the network which GRS to be in sleep mode. These parameters will be updated at regular intervals as well as whenever a new UAV enters the coverage area. While estimating whether a GRS goes to sleep mode or not, QoS constraints such as coverage and rate of UAV should be taken care of. Maintaining these QoS constraints, at any given point of time, following sleeping patterns are possible within a cluster of size n: $A_{n-1/n}, A_{n-2/n}, A_{n-3/n}, \ldots, A_{(n-(n-1))/n}$ which in general can be represented as $A_{n-i/n}$, where, $i = 1, 2, 3, \ldots, n-1$. $A_{n-i/n}$ means $n-i$ out of n GRSs operating in the cluster are in sleep mode. Let A_0 denote the nominal system where no GRS is in sleep mode. For example, in Fig. 2, Fig. 3, Fig. 4, and Fig. 5, we have considered a limited number of GRS sleeping patterns for a cluster size of 4. However, this framework can be extended to any number of possible GRS sleeping patterns. Fig. 2 corresponds to A_0 where all 4 GRSs in the cluster are active, Fig. 3 corresponds to $A_{3/4}$ scenario, Fig. 4 corresponds to $A_{2/4}$ scenario, and Fig. 5 corresponds to $A_{1/4}$ scenario. Next, we present the Utility function considered in this work.

G. UTILITY FUNCTION
The utility function for an α-Fair UAV scheduler with the variable x is expressed as [25]

$$U_\alpha(x) = \begin{cases} \dfrac{x^{1-\alpha}}{1-\alpha}, & \alpha > 0, \ \alpha \neq 1, \\ \log(x), & \alpha = 1. \end{cases} \tag{8}$$

Next, we present the performance metrics used to characterize the QoS in this work.

H. PERFORMANCE METRICS
There are three key performance metrics, namely, coverage probability, throughput, and energy efficiency considered in this work. The coverage probability is defined as the probability that a UAV u receives SINR $\gamma_{u,g}^m$ greater than the minimum SINR threshold S as specified in MCS [25] from at least one GRS g. We consider α-fair throughput over the set of UAVs and is expressed as follows [20].

$$T_\alpha = \begin{cases} \left(\dfrac{1}{|V_g|} \displaystyle\sum_{u \in V_g} R_u^{1-\alpha} \right)^{\frac{1}{1-\alpha}}, & \alpha > 0, \ \alpha \neq 1, \\ \left(\displaystyle\prod_{u \in V_q} R_u \right)^{\frac{1}{|V_g|}}, & \alpha = 1, \end{cases} \tag{9}$$

where, α is the fairness parameter, R_u as in (7), and V_g is the set of UAVs associated with the GRS g. We denote energy efficiency by $ES_{a1/a2}(\%)$ and it is defined as the percentage of energy saved via GRS sleeping. Each value of $ES_{a1/a2}(\%)$ corresponds to a particular GRSS pattern $A_{a1/a2}$. Let the energy consumed per unit time by a GRS be denoted by E. Then, nE is the energy consumed by the nominal system, A_0, since all n GRSs are on. The energy consumed E would be approximately constant irrespective of the number of UAVs associated with the GRS. Thus, a suitable measure of energy efficiency for a GRSS pattern $A_{a1/a2}$ in percentage when compared to the nominal system is given by [20].

$$ES_{a1/a2}(\%) = \frac{a1}{a2} \cdot 100, \tag{10}$$

where, $a1$ is the number of GRS sleeping and $a2$ is the total number of GRS considered. The joint optimization problem for resource allocation and energy efficiency is presented in the following section.

III. JOINT RESOURCE ALLOCATION AND ENERGY EFFICIENCY OPTIMIZATION
We consider $A_{a1/a2}$, the sleeping pattern as in Section II-F where, $a1$ is the number of GRSs sleeping and $a2$ is the total number of GRSs considered in the cluster. Similarly, the binary variable y_g denotes whether the GRS g is sleeping ($y_g = 0$) or active ($y_g = 1$). Let ξ_a and ξ_s denote the active and sleeping mode power consumption by GRS, respectively. Since we consider homogeneous GRSs, the power consumed ξ_a and ξ_s GRS are equal for all GRSs in the respective mode. The ξ_s is significantly smaller as compared to ξ_a. Further, we consider the data rate of every UAV u in the system should be greater than the operator fixed rate threshold τ_k. Given the binary association of UAV u with GRS g on the subchannel m, $y_{u,g}^m$ as in (5), SINR as in (2) at a time instant t, the joint resource allocation and energy efficiency problem

for a cluster k $(\mathcal{U}_k, \mathcal{G}_k)$ is formulated and presented as follows.

$$P1: \max_{\substack{\{x_{u,g}, y_g, \\ \tau_k, \beta_{u,g}\}}} \frac{\sum_{u \in \mathcal{U}} U_\alpha(R_u)}{\sum_{g \in \mathcal{G}} \left(y_g \xi_a + (1 - y_g) \xi_s \right)}, \tag{11}$$

$$\text{s.t.} \sum_{g \in \mathcal{G}_k} y_g \geq 1, \quad y_g \in \{0, 1\} \tag{12}$$

$$R_u = \sum_{g \in \mathcal{G}_k} x_{u,g} y_g \beta_{u,g} r_{u,g}, \quad \forall u \in \mathcal{U}_k, \tag{13}$$

$$R_u \geq \tau_k, \quad \forall u \in \mathcal{U}_k, \tag{14}$$

$$\sum_{u \in \mathcal{U}_k} y_g x_{u,g} \beta_{u,g} \leq 1, \quad \forall g \in \mathcal{G}_k \tag{15}$$

$$x_{u,g} = \begin{cases} 1, & \text{if } g = \arg\max_g \{y_g P_g^m h_{u,g}^m\}, \\ 0, & \text{otherwise}, \ \forall u \in \mathcal{U}_k, \ \forall g \in \mathcal{G}_k, \end{cases} \tag{16}$$

$$\gamma_{u,g}^m \geq S, \tag{17}$$

$$\beta_{u,g} \geq 0, \quad \forall u \in \mathcal{U}_k, \ \forall g \in \mathcal{G}_k, \tag{18}$$

where, (11) is the overall objective function for maximizing throughput and energy efficiency of the system with respect to the operator threshold τ_k and the UAV scheduling time constraint. (11) increases with increase in the utility function of the UAVs which in turn increases the throughput. Thus, (11) increases with increase in the throughput of the cluster. Since $\xi_s \leq \xi_a$, as more number of GRSs go into sleep mode, the denominator of (11) decreases, and thus, increasing the energy saved. Given the set of GRSs in cluster $\mathcal{G}_k$, the constraint on (12) specifies that at least one GRS should be active in the cluster k. The data rate of the particular UAV u is computed in (13) and the minimum rate constraint on the UAV's data rate R_u is specified in (14). Every cluster k can have its own rate threshold τ_k. If each UAV in the system has the data rate R_u greater than its corresponding τ_k, then GRS sleeping in a particular pattern is feasible. Otherwise, all GRS are active over the cluster to maintain the QoS of UAVs. The overall time fraction allocated to associated UAVs with the GRS g should not exceed one and it is shown in constraint (15). The UAV association is subject to change with every GRS sleeping pattern. Therefore, the constraint on UAV's association with only active GRS is given in (16). The constraint in (17) specifies that the SINR of UAV $\gamma_{u,g}^m$ should be greater than certain threshold S, i.e., no UAV should lose coverage after GRSS. The SINR and the positive time constraint are specified in (2) and (18), respectively. The overall system problem can be solved for a cluster. However, the same optimization problem formulated is applicable for all the clusters with varying cluster size. The given Problem **P1** in (11) is mixed-integer non-linear programming (MINLP) problem and is hard to solve in real-time for the binary variable y_g, discrete rate threshold τ_k, and the UAV scheduling time fraction $\beta_{u,g}$. Therefore, the problem is decomposed into UAV scheduling problem and joint UAV scheduling with GRS sleeping problem. Given the GRS sleeping pattern $A_{a1/a2}$, i.e., y_g, the decomposed UAV scheduling problem formulated for a cluster k with QoS

threshold τ_k is as follows.

$$P2: \max_{\beta_{u,g}} \sum_{u \in \mathcal{U}_k} U_\alpha(R_u), \tag{19}$$

$$\text{s.t. (13), (15), (16), (17), (18).} \tag{20}$$

The decomposed optimization problem in (19) is convex with respect to the variable $\beta_{u,g}$. This can be solved using Karush-Kuhn-Tucker (KKT) [26] method using the Lagrangian function given as follows.

$$L = -\sum_{u \in \mathcal{U}_k} \frac{1}{1 - \alpha} \left(\sum_{g \in \mathcal{G}_k} x_{u,g} y_g \beta_{u,g} r_{u,g} \right)^{1 - \alpha}$$
$$+ \sum_{g \in \mathcal{G}_k} \left(\sum_{u \in \mathcal{U}_k} Y_g x_{u,g} y_g \beta_{u,g} - 1 \right)$$
$$- \sum_{u \in \mathcal{U}_k} \sum_{g \in \mathcal{G}_k} D_{u,g} \beta_{u,g}. \tag{21}$$

The KKT conditions necessary to find the optimal solution for the aforementioned problem are as follows.

$$\frac{dL}{d\beta_{u,g}} = 0, \tag{22}$$

$$\sum_{g \in \mathcal{G}_k} \left(\sum_{u \in \mathcal{U}_k} Y_g x_{u,g} y_g \beta_{u,g} - 1 \right) = 0, \tag{23}$$

$$D_{u,g} \beta_{u,g} = 0, \tag{24}$$

where, (22) is the first-order necessary condition for optimal $\beta_{u,g}$. The complementary-slackness conditions are specified in (23) and (24). Applying (21) in (22), we get

$$-\sum_{u \in \mathcal{U}_k} \beta_{u,g}^{-\alpha} x_{u,g} r_{u,g}^{1-\alpha} + Y_g - D_{u,g} = 0, \tag{25}$$

$$\sum_{u \in \mathcal{U}_k} \beta_{u,g}^{-\alpha} x_{u,g} r_{u,g}^{1-\alpha} = Y_g - D_{u,g}. \tag{26}$$

The optimal $\beta_{u,g}$ should satisfy the condition $\beta_{u,g} > 0$ as in (18) and the complementary-slackness condition as in (24). Therefore, we consider $D_{u,g} = 0$ in (26) and on further simplification,

$$\beta_{u,g} = \frac{\left(x_{u,g} y_g r_{u,g} \right)^{\frac{1-\alpha}{\alpha}}}{Y_g^{\frac{1}{\alpha}}}. \tag{27}$$

Substituting (27) in (15), we get,

$$Y_g^{\frac{1}{\alpha}} = \sum_{u \in \mathcal{U}_k} x_{u,g} y_g r_{u,g}^{\frac{1-\alpha}{\alpha}}. \tag{28}$$

On substituting (28) in (27), the optimal $\beta_{u,g}$ is

$$\beta_{u,g}^* = \frac{x_{u,g} y_g r_{u,g}^{\frac{1-\alpha}{\alpha}}}{\sum_{u \in \mathcal{U}_k} x_{u,g} y_g r_{u,g}^{\frac{1\alpha}{\alpha}}}. \tag{29}$$

The similar UAV scheduler for $\alpha = 1$ is computed by maximizing $\sum_{u \in \mathcal{U}} \log(R_u)$ in the objective function as in (8). The proportionally fair UAV scheduling time fraction with $\alpha = 1$ is written as follows.

$$\beta_{u,g}^* = \frac{x_{u,g} y_g}{\sum_{u \in \mathcal{U}} x_{u,g} y_g}. \tag{30}$$

Given this UAV scheduling time fraction, the joint UAV scheduling with GRS sleeping problem is presented as follows.

$$P3 \quad \min_{y_g} \sum_{g \in \mathcal{G}} y_g, \tag{31}$$

$$\text{s.t. } (12), (16), (17), (30), \tag{32}$$

$$R_u = \sum_{g \in \mathcal{G}} x_{u,g} y_g \beta_{u,g}^* r_{u,g}, \quad \forall u \in \mathcal{U}_k, \tag{33}$$

where, the objective function in (31) is minimizing the number of active GRS. This is equivalent to maximizing the number of GRSs sleeping. (33) computes the data rate of the UAV u over the active GRS using the (30). The data rate of the UAV u should be greater than the threshold τ_k. We use the optimal $\beta_{u,g}^*$ computed in (30) for our GRS sleeping problem. Since y_g is binary, in order to find the GRSS pattern with maximum energy savings, we need to check for all possible combinations of y_g in the set $\mathcal{G}_k$. UAVs are subjected to varying mobility conditions. This varying mobility leads to varying QoS due to GRS sleeping. Thus, we next evaluate CoMP and NOMA for enhanced coverage and throughput, respectively, during GRSS.

IV. COORDINATED MULTI-POINT

Coordinated multi-point with the joint transmission which hereafter is referred to as CoMP is a proven technology to enhance coverage and provide better QoS in cellular scenario [20]. This is the motivation to consider CoMP along with the GRSS. We consider that the GRSs in a cluster can cooperate and perform CoMP [20]. Let each cluster formed while clustering the GRS be CoMP clusters as well. Without loss of generality, we focus on cluster k. The set of UAVs and GRSs in cluster k is $\mathcal{U}_k$ and $\mathcal{G}_k$, respectively.

We consider that the CoMP based system allocates a fraction of resources to CoMP UAVs in which all the GRSs within the CoMP cluster transmit jointly on the downlink to the CoMP UAVs. Whenever a UAV u in the CoMP cluster k receives the SINR less than a predetermined threshold denoted by χ then that UAV is served as a CoMP UAV. Let the time fraction in which all the GRSs within the CoMP cluster k transmit jointly on the downlink be denoted by θ_k. Then $(1 - \theta_k)$ will be the time fraction in which the GRSs serve their corresponding non-CoMP UAVs individually. Note that each CoMP cluster k can have its own θ_k.

Let $\mathcal{U}_{k,c}$ and $\mathcal{U}_{k,nc}$ denote the set of CoMP and non-CoMP UAVs in the cluster k. The SINR received by the CoMP UAV u, where, $u \in \mathcal{U}_{k,c}$ in the downlink time fraction θ_k from the

CoMP cluster k over the sub-channel m is denoted by $\gamma_{u,k}^m$ and given by

$$\gamma_{u,k,c}^m = \frac{\sum_{l \in \mathcal{G}_k} P_l^m h_{u,l}^m}{\sum_{\substack{\hat{l} \in \mathcal{G} \\ \hat{l} \notin \mathcal{G}_k}} P_{\hat{l}}^m h_{u,\hat{l}}^m + \sigma^2}, \tag{34}$$

where, $\sum_{l \in \mathcal{G}_k} P_l^m h_{u,l}^m$ is the power received by the UAV u from all GRSs in the CoMP cluster, k and $\sum_{\substack{\hat{l} \in \mathcal{G} \\ \hat{l} \notin \mathcal{G}_k}} P_{\hat{l}}^m h_{u,\hat{l}}^m$ is the interference from all other GRSs in the system which are not part of CoMP cluster k. Similarly, the SINR of non-CoMP UAVs in the cluster k is computed as in (2).

The link rate for the CoMP UAV is computed as follows.

$$r_{u,k} = \frac{\eta(\gamma_{u,k}^m) SC_{OFDM} SY_{OFDM}}{T_{sc}} \text{M.} \tag{35}$$

Similarly, the link rate of non-CoMP UAVs is computed as in (6). The resultant data rates of the CoMP UAV u in cluster k based on [20] is given as

$$R_u = \theta_k \beta_{u,k} r_{u,k}, \quad \forall u \in \mathcal{U}_{c,k}, \tag{36}$$

where, θ_k is the total CoMP time fraction available for all CoMP UAVs in the cluster k, $\beta_{u,k}$ is the UAV scheduling time fraction allocated for a CoMP UAV u by the cluster k, and $r_{u,k}$ is the link rate as in (35). The optimal UAV scheduling time fraction $\beta_{u,k}$ allocated to a CoMP UAV u by the cluster k as in [20] is given as follows.

$$\beta_{u,k} = \frac{r_{u,k}^{\frac{1-\alpha}{\alpha}}}{\sum_{u \in \mathcal{U}_{c,k}} r_{u,k}^{\frac{1-\alpha}{\alpha}}},$$

Similarly, the optimal CoMP time fraction for a cluster k, θ_k based on [20] is

$$\theta_k = \frac{\left(\sum_{u \in U_{c,k}} \beta_{u,k} r_{u,k} \right)^{\frac{1}{\alpha}}}{\left(\sum_{u \in U_{nc,k}} \sum_{g \in G_k} \beta_{u,g} r_{u,g} \right)^{\frac{1}{\alpha}} + \left(\sum_{u \in U_{c,k}} \beta_{u,k} r_{u,k} \right)^{\frac{1}{\alpha}}}.$$

The resultant rate of non-CoMP UAV u from GRS g is given as follows.

$$R_u = (1 - \theta_k) \sum_{g \in \mathcal{G}_k} x_{u,g}^m \beta_{u,g} r_{u,g}, \quad \forall u \in \mathcal{U}_{nc,k}, \tag{37}$$

where, $x_{u,g}^m$, $\beta_{u,g}$, and $r_{u,g}$ are computed as in (5), (29), and (6), respectively.

Next, we present the other key technology, Non-orthogonal multiple access (NOMA) considered in this work.

V. NON-ORTHOGONAL MULTIPLE ACCESS

High throughput and spectral efficiency are two key aspects that motivated us to look into Non-orthogonal multiple access (NOMA). When a GRS is in sleep mode there will be some loss in the coverage and throughput. The coverage is compensated by CoMP while the throughput can be compensated by adopting NOMA. We consider a NOMA system [21] for all GRSs where superposition coding (SC) is used to multiplex the signals of UAVs associated with a GRS and assume successive interference cancellation (SIC) is implemented at the receivers to separate the signals. Without loss of generality, we consider the kth cluster. For each GRS g in the kth cluster, let N_g be the number of UAVs associated with it. For NOMA, all the UAVs are sorted with respect to their channel gains as $|h^m_{u_1,g}|^2 > |h^m_{u_2,g}|^2 > |h^m_{u_3,g}|^2 > \ldots > |h^m_{u_{N_g},g}|^2$. Given this arrangement, the UAVs are divided into two groups. Let $\mathcal{U}_{k,g}$ be the set of UAVs associated with GRS g in cluster k. $\mathcal{U}^1_{k,g}$ be the first group of UAVs and $\mathcal{U}^2_{k,g}$ be the second group of UAVs. If N_g is even, then $\mathcal{U}^1_{k,g} = \{1, 2, 3, \ldots, N_g/2\}$ and $\mathcal{U}^2_{k,g} = \{N_g/2 + 1, N_g/2 + 2, N_g/2 + 3, \ldots, N_g/2 + N_g/2\}$. The pairing is such that UAV 1 from $\mathcal{U}^1_{k,g}$ is paired with lowest channel gain UAV which is nothing but $(N_g/2)^{th}$ UAV in the set $\mathcal{U}^2_{k,g}$, UAV 2 from $\mathcal{U}^1_{k,g}$ is paired with $(N_g/2 - 1)^{th}$ UAV in the set $\mathcal{U}^2_{k,g}$ and so on. In this way, all UAVs from $\mathcal{U}^1_{k,g}$ are paired with the UAVs in the $\mathcal{U}^2_{k,g}$. Thus, all UAVs associated with the GRS g are paired when N_g is even. Similarly, when N_g is odd $\mathcal{U}^1_{k,g} = \{1, 2, 3, \ldots, \lfloor N_g/2 \rfloor\}$, $\mathcal{U}^2_{k,g} = \{\lfloor N_g/2 \rfloor + 1, \lfloor N_g/2 \rfloor + 2, \lfloor N_g/2 \rfloor + 3, \ldots, \lfloor N_g/2 \rfloor + \lceil N_g/2 \rceil\}$, where UAV pairing is the same as before. The only difference is that, the $\lceil (N_g/2)^{th} \rceil$ UAV is left unpaired. This will be served as OMA UAV.

Let a NOMA pair be denoted by the ordered pair (p, q) where, $p \in \mathcal{U}^1_{k,g}$ and $q \in \mathcal{U}^2_{k,g}$. Let $\mathcal{N}_g$ denote the set of all NOMA ordered pairs associated with GRS g. When N_g is odd, the unpaired UAV is not included in the set $\mathcal{N}_g$ and such UAV be denoted by $N_{0,g}$. Hence, $\mathcal{N}_g = \{(p1, q1), (p2, q2), \ldots, (p\lfloor N_g/2 \rfloor, q\lceil N_g/2 \rceil)\}$. Let B denote the number of pairs formed for the GRS g in cluster k.

Here, we consider *P-NOMA*, where GRS allocates power to each NOMA pair based on their channel gains. In a pair, the UAV with a larger channel gain is allocated lesser power in comparison to the UAV with a small channel gain. Thus, both UAVs receive the superimposed signal from the GRS g. The SINR of the strong UAV p in the b^{th}NOMA pair over sub-channel m is given as

$$\gamma^m_{p,b,g} = \frac{\zeta_b P^m_g h^m_{p,g}}{\sum\limits_{\hat{g} \in \mathcal{G} \setminus g} P^m_{\hat{g}} h^m_{p,\hat{g}} + \sigma^2}, \tag{38}$$

where, the power from the GRS g over a sub-channel m, P^m_g is given in (1), the channel gain $h^m_{p,g}$ is given in (3), $\sum\limits_{\hat{g} \in \mathcal{G} / g} P^m_{\hat{g}} h^m_{p,\hat{g}}$ is the aggregate interference received by the UAV p on the sub-channel m from all other GRSs, and ζ_b is the fraction of total power allocated to higher channel gain UAV by the GRS g in NOMA pair b. We need to note that UAVs in a

b^{th} NOMA pair share same resources in time domain and successive interference cancellation is done at strong UAV, i.e., p^{th} UAV. Similarly, the SINR for weak UAV q in the same NOMA pair b is given as follows.

$$\gamma^m_{q,b,g} = \frac{(1 - \zeta_b)P^m_g h^m_{q,g}}{\zeta_b P^m_g h^m_{q,g} + \sum\limits_{\hat{g} \in \mathcal{G} \setminus g} P^m_{\hat{g}} h^m_{q,\hat{g}} + \sigma^2}, \tag{39}$$

where, $h^m_{q,g}$ is the channel gain of the weak UAV in the bth noma pair, σ^2 is the noise power, $\sum\limits_{\hat{g} \in \mathcal{G} \setminus g} P^m_{\hat{g}} h^m_{q,\hat{g}}$ is the interference received by the weak UAV from all other GRSs, and $(1 - \zeta_b)$ is the total power fraction assigned to the weak UAV in the bth NOMA pair. Given the SINR of strong UAV p and weak UAV q, the link rate, $r^b_{u,g}$ of the respective UAVs are computed based on (6). The resultant data rate of UAV u with NOMA based on [21] is given as follows.

$$R_u = \sum_{g \in \mathcal{G}} x^b_{u,g} \beta^b_{u,g} r^b_{u,g}, \tag{40}$$

where, $\beta^b_{u,g}$ is the time fraction allocated to the bth NOMA pair by GRS g and $r^b_{u,g}$ is the link rate of the UAV u in b^{th} NOMA pair by GRS g. The optimal UAV scheduling time fraction $\beta^b_{u,g}$ allocated to the bth NOMA pair by GRS g for $\alpha = 1$ based on [21] is given as follows.

$$\beta^b_{u,g} = \frac{1}{\sum\limits_{u \in \mathcal{U}} x^0_{u,g} + \sum\limits_{b \neq 0, b \in \mathcal{N}_g} \prod\limits_{u \in \mathcal{U}_{g,b}} x^b_{u,g}},$$

where, $\mathcal{U}_{g,b}$ is the set of UAVs associated with GRS g present in b^{th} NOMA pair, $\sum\limits_{b \neq 0, b \in \mathcal{N}_g} \prod\limits_{u \in \mathcal{U}_{g,b}} x^b_{u,g}$ is the total number of UAVs in the NOMA pair b, and $x^0_{u,g}$ is binary variable represents the association of unpaired UAV u in GRS g. The optimal power allocation scheme for ζ_b has been discussed in [27] for cellular scenario and the same can be applied here.

In the following section, we propose three algorithms to dynamically solve the problem mentioned in (31).

VI. DYNAMIC GRS SLEEPING ALGORITHM WITH UAV MOBILITY

We propose a Dynamic GRS sleeping algorithm for the UAV network which simultaneously ensures energy efficiency and coverage. The presented optimization problems in (11), (19), and (31) are for a time instant t, whereas, UAV's position varies with every time instant t. The decision of GRS sleeping is taken based on QoS constraint as in (14) and (17). The proposed dynamic sleeping algorithm is hereby illustrated for the cluster k. However, the same can be applied to all the clusters. This algorithm searches for the sleeping pattern $A^{t,*}_{a1/a2}$ which maximizes the energy savings at time instant t while ensuring that the QoS constraints in (14) and (17) are satisfied.

Each GRS in the cluster estimates the SINR of UAVs associated with it at discretized (with step size δ) time intervals and shares this information with the GCS. The step size δ can be varied up to the desired accuracy level. Let the SINR

Algorithm 1 Dynamic GRS Sleeping

1: INPUTS: $\{P_g^m, h_{u,g}^m, \eta(\gamma_{u,g}), M, \mathcal{U}_k, \mathcal{G}_k, V_u, \tau, \{A_{a1/a2}^j\}, S\}$

2: OUTPUTS: $A_{a1/a2}^{(t,*)}$

3: Sort $A_{a1/a2}$ in the descending order of energy saved

4: Initialize: $J = |\{A_{a1/a2}^j\}|$, $A_{a1/a2}^{t,*} = A_{a1/a2}^1$, $j = 1$

5: **while** $j \leq J$ **do**

6:     Calculate $\Phi_{a1/a2}$, $\Gamma_{a1/a2}$

7:     $\gamma_{u,g} = f(\{P_g^m h_{u,g}^m\})$ $\forall u \in \mathcal{U}_k$, as in (2)

8:     $R_u = f(\{\eta(\gamma_{u,g})M\})$ $\forall u \in \mathcal{U}_k$, as in (7)

9:     **if** $\forall$ u s.t $R_u \geq \tau_k$ & $\forall$ u s.t $\gamma_{u,g} \geq S$ **then**

10:         $A_{a1/a2}^{(t,*)} = A_{a1/a2}^j$

11:         **break**

12:     **else if** $j == J$ **then**

13:         $A_{a1/a2}^{(t,*)} = A_0$

14:     **else**

15:         $j = j + 1$

16:     **end if**

17: **end while**

Algorithm 2 Dynamic GRS Sleeping With CoMP

1: INPUTS: $\{P_g^m, h_{u,g}^m, \eta(\gamma_{u,g}), M, \mathcal{U}_k, \mathcal{G}_k, V_u, \tau, \{A_{a1/a2}^j\},$

2: OUTPUTS: $A_{a1/a2}^{(t,*)}$

3: Sort $A_{a1/a2}$ in the descending order of energy saved

4: Initialize: $J = |\{A_{a1/a2}^j\}|$, $A_{a1/a2}^{t,*} = A_{a1/a2}^1$, $j = 1$

5: **while** $j \leq J$ **do**

6:     Calculate $\Gamma_{a1/a2}$

7:     $\gamma_{u,g} = f(\{P_g^m h_{u,g}^m\})$ $\forall u \in \mathcal{U}_k$ as in (2)

8:     **if** $\exists$ $\gamma_{u,g} < S \in \Gamma_{a1/a2}$ & $j < J$ **then**

9:         Calculate $\gamma_{u,g} = f(\{P_g^m h_{u,g}^m\})$ as in (34) and (2) denoted as $\hat{\Gamma}_{a1/a2}$

10:         Calculate $R_u = f(\{\eta(\gamma_{u,g})M\})$ as in (36) $\forall u \in \mathcal{U}_k$, denoted as $\hat{\Psi}_{a1/a2}$

11:         **if** $\exists$ u s.t $\hat{\Gamma}_{a1/a2} < S$ or $\hat{\Psi}_{a1/a2} < \tau_k$ **then**

12:             $j = j + 1$

13:         **else if** $\hat{\Gamma}_{a1/a2} \geq S$ & $\hat{\Psi}_{a1/a2} \geq \tau_k$ **then**

14:             $A_{a1/a2}^{(t,*)} = A_{a1/a2}^j$

15:             **break**

16:         **end if**

17:     **else**

18:         Calculate $\Phi_{a1/a2}$

19:         $R_u = f(\{\eta(\gamma_{u,g})M\})$ $\forall u \in \mathcal{U}_k$, as in (7)

20:         **if** $\forall$ u s.t $R_u \geq \tau_k$ **then**

21:             $A_{a1/a2}^{(t,*)} = A_{a1/a2}^j$

22:             **break**

23:         **else if** $j == J$ **then**

24:             $A_{a1/a2}^{(t,*)} = A_0$

25:         **else**

26:             $j = j + 1$

27:         **end if**

28:     **end if**

29: **end while**

---

vector of UAVs associated with cluster k at time t be $\Gamma_{\Omega \times 1}$. With this SINR vector, rates of UAVs are calculated using (6) and (7). Let that rate vector be $\Psi_{\Omega \times 1}$.

The GRS computes an estimate of SINR vector $\Gamma_{a1/a2}$ and the corresponding rate vector $\Psi_{a1/a2}$ using (2) and (7), respectively, for different sleeping patterns at each time instant t. The proposed algorithm searches for a GRS sleeping pattern in the descending order of their energy saving. Hence, initially, these vectors are calculated for $A_{n-1/n}$ configuration as this configuration results in the maximum energy savings. If no UAV loses coverage, i.e., no element of the SINR vector $\Gamma_{a1/a2}$ should be less than S dB, then the corresponding rate vector $\Psi_{a1/a2}$ is calculated. In case the rate of no UAV doesn't drop below the threshold τ_k, i.e., no element of the vector $\Psi_{a1/a2}$ should be less than τ_k, then this sleeping configuration is optimal for the time instant t, i.e., $A_{a1/a2}^{t,*} = A_{n-1/n}$. If either of the aforementioned conditions (QoS constraints) fail, then the $\Gamma_{a1/a2}$ and $\Psi_{a1/a2}$ are updated for the next maximum energy savings configuration, i.e., $A_{n-2/n}$. In case $A_{n-2/n}$ configuration also doesn't satisfy the above conditions, then the algorithm checks for $A_{n-3/n}$ configuration. In this way, the algorithm checks until the configuration, $A_{1/n}$ if the configurations $A_{n-1/n}$ to $A_{n-(n-2)/n}$ fail to satisfy the QoS constraints. If the configuration $A_{1/n}$ also fails to satisfy the QoS constraints, then the algorithm gives the output as A_0, i.e., no sleeping is possible and all GRS in the cluster should be active. Whenever a new UAV enters or leaves the coverage area of the GCS, Ω gets updated and at the same time all other parameters mentioned in the algorithm are recomputed. The proposed algorithm is presented in Algorithm 1. Next, we present Dynamic GRS algorithm with CoMP considered in this paper.

A. DYNAMIC GRS SLEEPING WITH CoMP

The GRS sleeping can result in energy saving at the cost of coverage and UAV's data rate. Given any GRSS pattern $A_{a1/a2}$, UAVs SINR and data rate are computed as in (2) and (7), respectively. If any of the UAV's SINR falls below the threshold S, then we perform CoMP for cluster k. The updated SINR vector $\hat{\Gamma}_{a1/a2}$ is computed as in (34) and (2). In case SINR of any UAV in the $\hat{\Gamma}_{a1/a2}$ is below the threshold S, then the heuristic presented in Algorithm 2 increments the value of j (index of the GRSS pattern after sorting the patterns in the descending order of their energy savings as shown in Algorithm 1 and Algorithm 2) and check for the next GRSS pattern. If the SINR of all UAVs is above the threshold S, then the updated rate vector $\hat{\Psi}_{a1/a2}$ is computed with CoMP as in [20]. Thus, the heuristic now considers the updated rate vector $\hat{\Psi}_{a1/a2}$ for the selection of configuration $A_{a1/a2}$. Please note that CoMP is performed only if at least two GRSs are active. For example, CoMP is not applicable for the

Algorithm 3 Dynamic GRS Sleeping With NOMA

1: INPUTS: $\{P_g^m, h_{u,g}^m, \eta(\gamma_{u,g}), M, \mathcal{U}_k, \mathcal{G}_k, V_u, \tau, \{A_{a1/a2}^j\}, S\}$

2: OUTPUTS: $A_{a1/a2}^{(t,*)}$

3: Sort $A_{a1/a2}$ in the descending order of energy saved

4: Initialize: $J = |\{A_{a1/a2}^j\}|$, $A_{a1/a2}^{t,*} = A_{a1/a2}^1$, $j = 1$

5: **while** $j \leq J$ **do**

6:     Calculate $\Phi_{a1/a2}, \Gamma_{a1/a2}$

7:     $\gamma_{u,g} = f(\{P_g^m h_{u,g}^m\})\ \forall u \in \mathcal{U}_k$, as in (2)

8:     $R_u = f(\{\eta(\gamma_{u,g})M\})\ \forall u \in \mathcal{U}_k$, as in (7)

9:     **if** $\forall u$ s.t $R_u \geq \tau_k$ & $\forall u$ s.t $\gamma_{u,g} \geq S$ **then**

10:         $A_{a1/a2}^{(t,*)} = A_{a1/a2}^j$

11:         Calculate $\tilde{\Gamma}_{a1/a2}\ \forall u \in \mathcal{U}_k$, as in (38) & (39)

12:         Calculate $\tilde{\Psi}_{a1/a2}\ \forall u \in \mathcal{U}_k$, as in (40)

13:         **break**

14:     **else if** $j == J$ **then**

15:         $A_{a1/a2}^{(t,*)} = A_0$

16:         Calculate $\tilde{\Gamma}\ \forall u \in \mathcal{U}_k$, as in (38) & (39)

17:         Calculate $\tilde{\Psi}\ \forall u \in \mathcal{U}_k$, as in (40)

18:     **else**

19:         $j = j + 1$

20:     **end if**

21: **end while**

TABLE 3. Simulation parameters.

B, Environment constant, Dense Urban	0.136
C, Environment constant, Dense Urban	11.95
Cluster Size of GRSs	4
h_0, Altitude of the UAV (m)	542
M, Number of subchannels	15
P_g^m, power allocated per subchannel in dBm	34.2391
S, SINR Threshold (dB)	-6.5
SC_{OFDM}, subcarriers/channel	12
SY_{OFDM}, number of symbols used/subcarrier	14
Standard deviation of shadowing random variable (dB)	2.6 dB
ν, Velocity of UAV (m/sec)	[32, 120]
f_L (GHz), L-band frequency	0.968
m, Nakagami - m parameter	6
Time intervals	500
ζ_b, Fraction of power allotted to strong UAV for b^{th} NOMA pair	0.25
α_L, Pathloss exponent for LOS link	4
α_N, Pathloss exponent for NLOS link	2.5
δ (in sec), Step size	1
λ_G (GRSs/km^2), Density of ground radio stations	$\{6, 8, 10, 12, 14\}$
λ_u (UAVs/km^2), Density of UAVs	$\{10, 20, 30, 40, 50, 60, 70, 80, 90, 100\}$
τ_k (bits/sec), Rate threshold	50×10^3

configuration in Fig. 3. The detailed algorithm for dynamic GRS sleeping with CoMP is presented in Algorithm 2. In the following subsection, we present dynamic GRS sleeping with NOMA.

B. DYNAMIC GRS SLEEPING WITH NOMA

After sleeping configuration is determined using either Algorithm 1 (without CoMP) or Algorithm 2 (with CoMP), i.e., given the GRSS pattern $A_{a1/a2}^{t,*}$, the UAVs in the cluster k are paired based on Section V using NOMA. In this work, NOMA pairing is done without considering CoMP while determining the appropriate sleeping configuration. Please note that the UAVs that are associated only with the GRSs in cluster k are paired using NOMA. Given the NOMA UAV pairing, the SINR and data rate of UAVs for NOMA are computed as in (38), (39), and (40), respectively. The throughput of the system with NOMA is now computed using this updated SINR vector $\tilde{\Gamma}_{a1/a2}$ and rate vector $\tilde{\Psi}_{a1/a2}$. The detailed algorithm is presented in Algorithm 3. Given the GRSS pattern, the inclusion of CoMP and NOMA increases coverage and the throughput of the system, respectively. The detailed numerical results for the three algorithms are presented next.

VII. NUMERICAL RESULTS

In this section, we present numerical results to validate our analysis. We first verify the average throughput of the benchmark system for various λ_u and λ_g. We then show that considering CoMP along with the benchmark system results
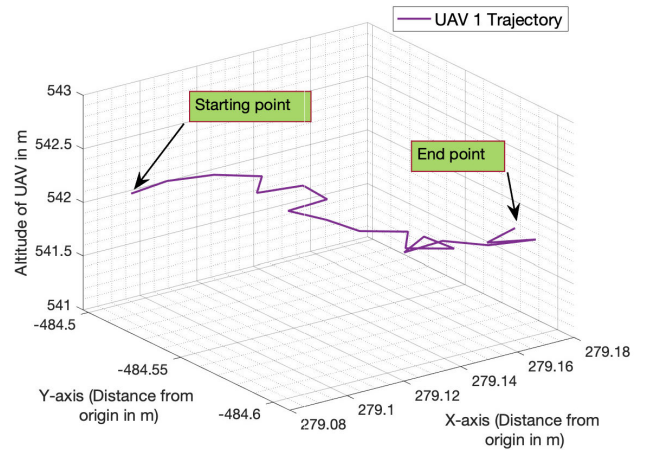

FIGURE 6. A part of the trajectory of a UAV generated using Random mobility model.

in an increase of coverage at the expense of the decreased throughput. We also present the results for NOMA along with the benchmark system and show that the average throughput of the system increases by considering NOMA. Further, we present the numerical results of the discussed algorithm for GRS sleeping. The energy saved when GRS sleeping is performed with and without CoMP, and the corresponding throughput results are also presented. The increase in the throughput by adding NOMA for GRS sleeping is also presented.

In this section, we do not directly compare the performance of the proposed algorithms with those of the existing works
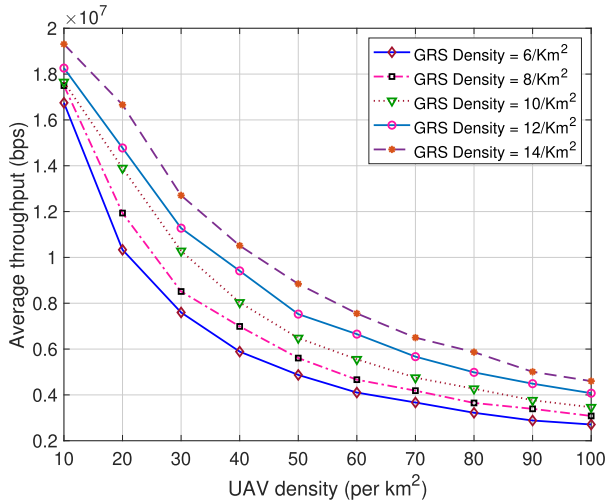
FIGURE 7. Throughput for varying λ_u given $\lambda_g = \{6, 8, 10, 12, 14\}$ per km^2 for Benchmark system.

FIGURE 8. Throughput for varying λ_u when NOMA and CoMP are considered along with Benchmark system given $\lambda_g = 6/$ km^2.

on UAV communications. This is because the existing works on UAV communications [3]– [24] focused on channel modelling for CNPC links and did not study the infrastructure and energy consumption related issues. We present the advantages of the proposed framework in energy savings and the gain in throughput using Monte Carlo simulations performed using MATLAB_R2021a.

We consider a system where, GRSs are deployed randomly using Poisson point process (PPP) [20]. Results are plotted for multiple GRS densities, namely, {6, 8, 10, 12, 14} per km^2 and for multiple UAV densities, {10, 20, 30, . . . , 100} per km^2.The parameters used in the simulation are summarized in Table 3. The UAV densities and GRS densities are varied to study the impact of sleeping, NOMA, and CoMP on low, average, and high densities. An area of 10 km^2 is considered for the simulation. However, results presented focus on the center area of 1 km^2. The simulation for each GRS density and for each UAV density is averaged over 10^3 location realizations as well as fading and shadowing realizations. Simulation results are presented for the center cluster and the cluster size in the simulation is considered to be 4. Clustering of GRS is done based on the distance among the GRSs. Euclidean Distance from one GRS to the other GRSs is calculated and 3 GRSs which are close to the GRS from which distance has been calculated are grouped under one cluster [28]. We have ensured that a GRS doesn't belong to two or more clusters simultaneously.

The trajectory of all UAVs is calculated using the Random waypoint mobility model. Random waypoint mobility model [29] is defined as follows:

$$R(t) = \begin{cases} \theta(t), & (0, 2\pi], \\ v(t), & (0, v_{max}]. \end{cases} \quad (41)$$

In the Random waypoint mobility model, the nodes change their velocity and direction at each time interval. Here nodes represent UAVs and minimum velocity is not zero. Here
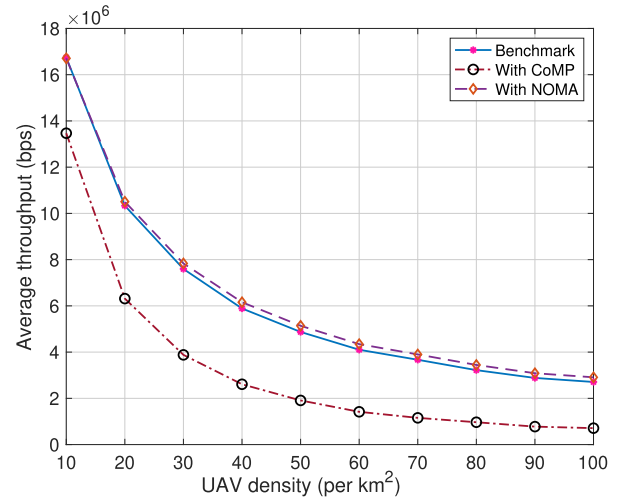
velocity ranges from 32 *m/s* to 120 *m/s*. It is assumed that each UAV moves with a uniform velocity which is chosen uniformly randomly from the range mentioned. At each time interval, *t* UAV chooses an angle from the set $(0, 2\pi]$ and moves in that direction with already chosen uniform velocity v. So, during this time interval, UAV moves with a velocity vector $(vcos\theta(t), vsin\theta(t))$. Following these rules, if any UAV moves out of the boundary then it is bounced back into the simulation field with an angle of $\pi - \theta(t)$. The random waypoint mobility model is a memoryless model. Hence, the current angle of the traverse is independent of the previous one. Fig. 6 shows a part of the trajectory of a UAV generated using a random mobility model.

The variation of throughput for different λ_g and λ_u are presented in Fig. 7. It is observed that for a particular λ_g by increasing λ_u throughput of the cluster is gradually decreasing. The increase in λ_u makes the α-fair scheduler allocate less fraction of time to each UAV and this attributes to the reduction in overall throughput of the cluster. However, by increasing the λ_g, the throughput curve is moving up which indicates the increase in the throughput of the system. Increasing the λ_g increases the overall time fraction allocated to each UAV due to which there is a rise in throughput of the system.

The throughput of the system is also calculated by considering NOMA and CoMP individually with GRSS. It is observed that the system performance in terms of throughput improves after using NOMA. On the other hand, CoMP improves coverage at an expense of decreased throughput. For a given λ_g and λ_u system with NOMA has more throughput than benchmark while the system with CoMP has less throughput than the benchmark. Fig. 8 shows the throughput variation of NOMA and CoMP comparing it with the benchmark system for $\lambda_g = 6/$ km^2. The throughput of the system when NOMA is considered is the highest because of the pairing between UAVs. Due to this pairing, more time fraction
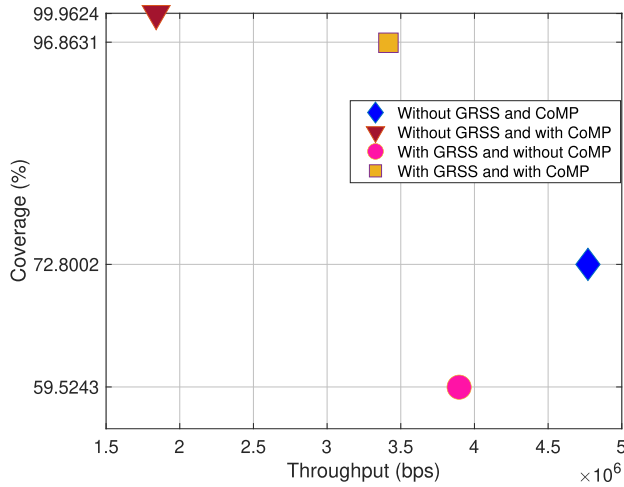
FIGURE 9. Illustration of coverage with/without CoMP and with/without GRSS for $\lambda_g = 6/$ km^2 and $\lambda_u = 50/$ km^2.
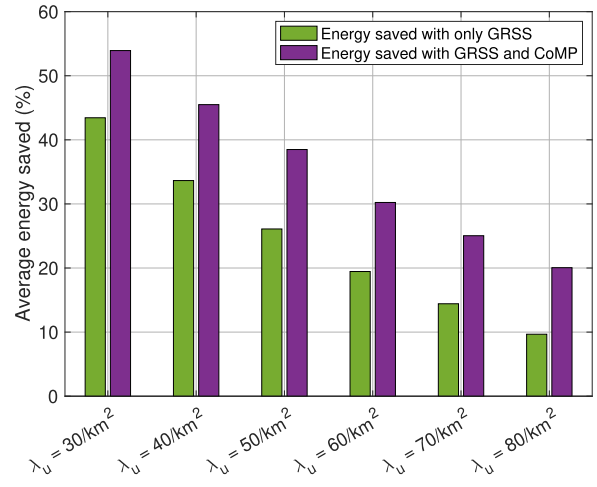

FIGURE 11. Illustration of energy savings with GRSS and with GRSS considering CoMP given $\lambda_g = 6/$ km^2.
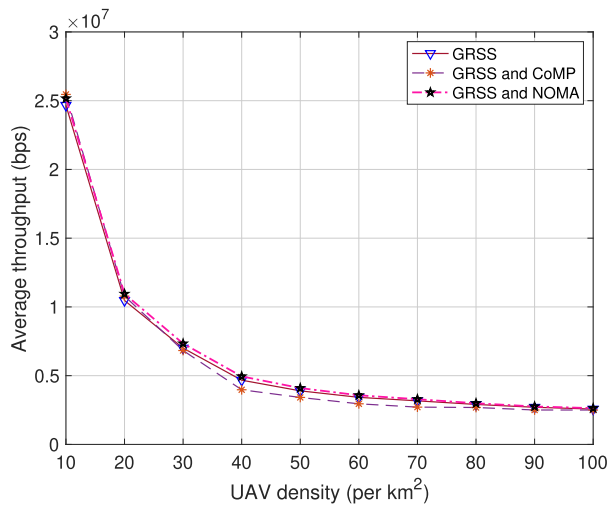

FIGURE 10. Throughput for varying λ_u for GRSS, GRSS with NOMA, and GRSS with CoMP given $\lambda_g = 6/$ km^2.
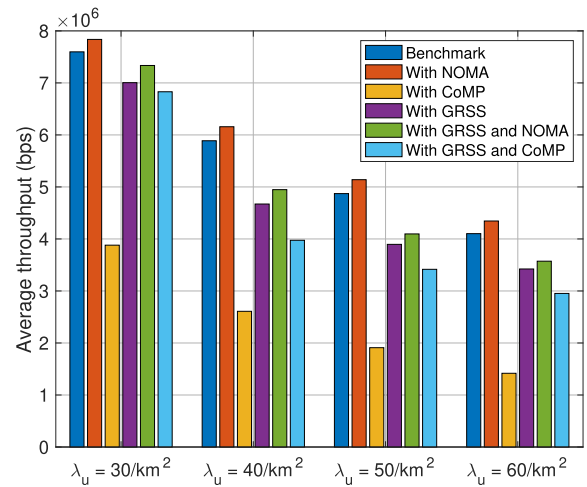

FIGURE 12. Illustration of throughput trade off for different scenarios given $\lambda_g = 6/$ km^2.

is available to each UAV to transmit its data than that of the benchmark system. When CoMP is considered, there is a system level requirement of CoMP and non-CoMP time fraction. This decreases the amount of time fraction available to each UAV when compared with that of benchmark system. Hence, the throughput of the system with CoMP is less than that of the benchmark system. As mentioned that CoMP increases the coverage, the result validating this observation is presented in Fig. 9. We can see that the coverage with CoMP in both cases is better than without CoMP. The coverage of the system with GRSS is less than that of the benchmark system because in the benchmark system, all the GRSs in the cluster are in active mode but when GRSS is considered, few GRSs in the cluster are in sleep mode. However, when CoMP is considered in both the systems, all active GRSs in the cluster jointly transmit the signal to UAVs whose SINR is below a certain threshold. Thus, more UAVs come into the coverage.

This is the reason for increased coverage of the CoMP based system in Fig. 9. Fig. 10 shows the trends of throughput when GRSS alone is performed, GRSS with NOMA, and GRSS with CoMP is performed. From the trends, it is observed that the throughput drop due to GRS sleeping can be compensated using NOMA. However, at lower UAV densities, it can be seen that there is no significant difference among the three curves in Fig. 10. with the increase in the UAV density NOMA gives better throughput.

Fig. 11 shows the energy savings. The advantage of CoMP during GRSS is seen in energy savings. It can be observed from the plot that average energy saved is decreasing with an increase in the UAV density for a constant GRS density. There are two energy saving bars shown against each UAV density. One bar is without CoMP and the other is with CoMP. Using CoMP while deciding GRS sleeping pattern, significantly increased the average energy savings but at a cost of slight reduction in the average throughput. For a

given GRS density, at lower UAV density, energy-saving with and without CoMP doesn't show much difference. However, there is an approximate difference of 10% seen as UAV densities reach 40 per km². At higher UAV densities GRSS with CoMP is shown to be more energy efficient. Hence, performing GRSS along with CoMP significantly increases energy savings. However, from the throughput perspective, NOMA is seen performing better even in GRSS.

Fig. 12 shows a detailed comparison of the average throughput of the benchmark system with NOMA, CoMP, with GRSS, with GRSS and NOMA, with GRSS and CoMP. From the bar graph in Fig. 12, it is observed that when GRSS is performed, the throughput of the system is dropped and thereby applying NOMA has compensated a part of the throughput drop. The order of the throughput seen is Benchmark with NOMA ≥ Benchmark ≥ GRSS with NOMA ≥ GRSS ≥ GRSS with CoMP ≥ Benchmark with CoMP. The throughput of the Benchmark system with CoMP is less than the throughput of the system with GRSS and CoMP because after GRS sleeping some UAVs are offloaded to the other clusters. Hence, the scheduling time fraction is increased for the remaining UAVs resulting in a higher throughput. The throughput of the benchmark system with CoMP is the least among all scenarios. However, CoMP significantly increases the coverage as seen in Fig. 9. On the other hand, the throughput of the benchmark system with NOMA is higher in all other scenarios. Motivated by this in future we plan to investigate a joint CoMP-NOMA system for UAV communications.
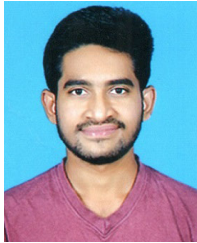
VIII. CONCLUSION

In this paper, we have proposed algorithms for maximizing the energy efficiency of the UAV infrastructure through a dynamic GRS sleeping subject to coverage and rate constraints. To the best of our knowledge, this is the first study of energy efficiency done in the area of CNPC links for UAV communication. We have formulated the GRS sleeping as an optimization problem. Then, we have proposed a dynamic GRS sleeping algorithm with UAV mobility to solve the optimization. We have demonstrated that the proposed algorithm achieves significant energy efficiency through numerical results. Further, we have shown that CoMP with GRSS achieves significant energy savings and NOMA compensates for the throughput loss due to GRSS.

REFERENCES

[1] Y. Zeng, R. Zhang, and T. J. Lim, "Wireless communications with unmanned aerial vehicles: Opportunities and challenges," *IEEE Commun. Mag.*, vol. 54, no. 5, pp. 36–42, May 2016.

[2] *5G Evolution and 6G*, NTT DOCOMO, Tokyo, Japan, 2021.

[3] B. Kerczewski, "Spectrum for UAS control and non-payload communications," in *Proc. Integr. Commun., Navigat. Surveill. Conf. (ICNS)*, Herndon, VA, USA, Apr. 2013, pp. 1–21.

[4] W. Khawaja, I. Guvenc, D. W. Matolak, U.-C. Fiebig, and N. Schneckenburger, "A survey of air-to-ground propagation channel modeling for unmanned aerial vehicles," *IEEE Commun. Surveys Tuts.*, vol. 21, no. 3, pp. 2361–2391, 3rd Quart., 2019.

[5] D. W. Matolak and R. Sun, "Air–ground channel characterization for unmanned aircraft systems—Part I: Methods, measurements, and models for over-water settings," *IEEE Trans. Veh. Technol.*, vol. 66, no. 1, pp. 26–44, Jan. 2017.

[6] R. Sun and D. W. Matolak, "Air–ground channel characterization for unmanned aircraft systems—Part II: Hilly and mountainous settings," *IEEE Trans. Veh. Technol.*, vol. 66, no. 3, pp. 1913–1925, Mar. 2017.

[7] D. W. Matolak and R. Sun, "Air–ground channel characterization for unmanned aircraft systems—Part III: The suburban and near-urban environments," *IEEE Trans. Veh. Technol.*, vol. 66, no. 8, pp. 6607–6618, Aug. 2017.

[8] W. Khawaja, I. Guvenc, and D. Matolak, "UWB channel sounding and modeling for UAV air-to-ground propagation channels," in *Proc. IEEE Global Commun. Conf. (GLOBECOM)*, Washington, DC, USA, Dec. 2016, pp. 1–7.

[9] W. Khawaja, O. Ozdemir, and I. Guvenc, "UAV air-to-ground channel characterization for mmWave systems," in *Proc. IEEE 86th Veh. Technol. Conf. (VTC-Fall)*, Toronto, ON, Canada, Sep. 2017, pp. 1–5.

[10] M. Ibrahim and H. Arslan, "Air-ground Doppler-delay spread spectrum for dense scattering environments," in *Proc. IEEE Mil. Commun. Conf. (MILCOM)*, Tampa, FL, USA, Oct. 2015, pp. 1661–1666.

[11] V. Vahidi and E. Saberinia, "Orthogonal frequency division multiplexing and channel models for payload communications of unmanned aerial systems," in *Proc. Int. Conf. Unmanned Aircr. Syst. (ICUAS)*, Arlington, VA, USA, Jun. 2016, pp. 1156–1161.

[12] L. Zhou, Z. Yang, S. Zhou, and W. Zhang, "Coverage probability analysis of UAV cellular networks in urban environments," in *Proc. IEEE Int. Conf. Commun. Workshops (ICC Workshops)*, Kansas City, MO, USA, May 2018, pp. 1–6.

[13] M. Alzenad and H. Yanikomeroglu, "Coverage and rate analysis for unmanned aerial vehicle base stations with LoS/NLoS propagation," in *Proc. IEEE Globecom Workshops (GC Wkshps)*, Abu Dhabi, United Arab Emirates, Dec. 2018, pp. 1–7.

[14] R. Jiang, K. Xiong, T. Liu, D. Wang, and Z. Zhong, "Coverage probability-constrained maximum throughput in UAV-aided SWIPT networks," in *Proc. IEEE Int. Conf. Commun. Workshops (ICC Workshops)*, Dublin, Ireland, Jun. 2020, pp. 1–6.

[15] B. Galkin, J. Kibilda, and L. A. Da Silva, "A stochastic model for UAV networks positioned above demand hotspots in urban environments," *IEEE Trans. Veh. Technol.*, vol. 68, no. 7, pp. 6985–6996, Jul. 2019.

[16] J. Qin, Z. Wei, C. Qiu, and Z. Feng, "Edge-prior placement algorithm for UAV-mounted base stations," in *Proc. IEEE Wireless Commun. Netw. Conf. (WCNC)*, Marrakesh, Morocco, Apr. 2019, pp. 1–6.

[17] C.-C. Lai, C.-T. Chen, and L.-C. Wang, "On-demand density-aware UAV base station 3D placement for arbitrarily distributed users with guaranteed data rates," *IEEE Wireless Commun. Lett.*, vol. 8, no. 3, pp. 913–916, Jun. 2019.

[18] M. Demirtas, F. Aydin, G. Tanis, and C. Arslan, "Indoor coverage analysis for unmanned aerial vehicle base stations," in *Proc. 27th Signal Process. Commun. Appl. Conf. (SIU)*, Sivas, Turkey, Apr. 2019, pp. 1–4.

[19] T. Sivalingam, K. B. S. Manosha, N. Rajatheva, M. Latva-Aho, and M. B. Dissanayake, "Positioning of multiple unmanned aerial vehicle base stations in future wireless network," in *Proc. IEEE 91st Veh. Technol. Conf. (VTC-Spring)*, Antwerp, Belgium, May 2020, pp. 1–6.

[20] Y. Ramamoorthi and A. Kumar, "Resource allocation for CoMP in cellular networks with base station sleeping," *IEEE Access*, vol. 6, pp. 12620–12633, Mar. 2018.

[21] G. Chopra, Y. Ramamoorthi, A. Kumar, and A. Dubey, "Non-orthogonal multiple access for ultra-dense cellular networks with base station sleeping," in *Proc. IEEE 3rd 5G World Forum (5GWF)*, Bangalore, India, Sep. 2020, pp. 596–601.

[22] H. W. Kim, K. Kang, K. Lim, and J. Y. Ahn, "Performance analysis for terrestrial radio waveform for control and non-payload communication of unmanned aircraft systems," in *Proc. Int. Conf. Inf. Commun. Technol. Converg. (ICTC)*, Jeju, South Korea, Oct. 2016, pp. 759–761.

[23] G. A. Wilkin and X. Huang, "*K*-means clustering algorithms: Implementation and comparison," in *Proc. 2nd Int. Multi-Symp. Comput. Comput. Sci. (IMSCCS)*, Iowa City, IA, USA, Aug. 2007, pp. 133–136.

[24] X. Wang, H. Zhang, and V. C. M. Leung, "Modeling and performance analysis of UAV-assisted cellular networks in isolated regions," in *Proc. IEEE Int. Conf. Commun. Workshops (ICC Workshops)*, Kansas City, MO, USA, May 2018, pp. 1–6.

[25] A. F. Molisch, *Wireless Communications*. New York, NY, USA: Wiley, 2005.

[26] S. Boyd and L. Vandenberghe, *Convex Optimization*. Cambridge, U.K.: Cambridge Univ. Press, 2004.

[27] L. Zhu, J. Zhang, Z. Xiao, X. Cao, and D. O. Wu, "Optimal user pairing for downlink non-orthogonal multiple access (NOMA)," *IEEE Wireless Commun. Lett.*, vol. 8, no. 2, pp. 328–331, Apr. 2019.

[28] D. Tian, Y. Wang, G. Lu, and G. Yu, "A VANETs routing algorithm based on Euclidean distance clustering," in *Proc. 2nd Int. Conf. Future Comput. Commun.*, 2010, pp. V1-183–V1-187.

[29] F. Bai and A. Helmy, "A survey of mobility modeling and analysis in wireless ad hoc networks," in *Wireless Ad Hoc and Sensor Networks*. Norwell, MA, USA: Kluwer, Jun. 2004.

ABHINAV KUMAR (Senior Member, IEEE) received the dual B.Tech. degree in electrical engineering, the M.Tech. degree in information and communication technology, and the Ph.D. degree in electrical engineering from the Indian Institute of Technology (IIT) Delhi, in 2009, 2009, and 2013, respectively. In 2013, he was a Research Associate with IIT Delhi. From 2013 to 2014, he was a Postdoctoral Fellow with the University of Waterloo, Canada. Since 2014, he has been with IIT Hyderabad, India, where he is currently an Associate Professor. His current research interests include different aspects of wireless communications and networking.

AKHILESWAR CHOWDARY (Graduate Student Member, IEEE) received the B.Tech. degree in electronics and communication engineering from Maulana Azad National Institute of Technology, Bhopal, in 2019. He is currently pursuing the M.Tech. degree in electrical engineering with the Indian Institute of Technology Hyderabad, India.

YOGHITHA RAMAMOORTHI (Member, IEEE) received the B.E. and M.E. degrees from Anna University, Chennai, India, in 2012 and 2014, respectively, and the Ph.D. degree from the Department of Electrical Engineering, Indian Institute of Technology Hyderabad, in 2020. She is currently a Postdoctoral Researcher at NTT Access Network Service Systems Laboratories, Yokosuka, Japan. Her research interests include intelligent reflecting surfaces, energy efficiency, resource allocation, and multi-connectivity technologies of next-generation wireless networks.

LINGA REDDY CENKERAMADDI (Senior Member, IEEE) received the master's degree in electrical engineering from the Indian Institute of Technology, New Delhi, India, in 2004, and the Ph.D. degree in electrical engineering from the Norwegian University of Science and Technology, Trondheim, Norway, in 2011. He worked with Texas Instruments in mixed-signal circuit design before joining the Ph.D. program at NTNU. After finishing the Ph.D., he worked in radiation imaging for an atmosphere space interaction monitor (ASIM mission to International Space Station) with the University of Bergen, Norway, from 2010 to 2012. He is currently working as an Associate Professor with the University of Agder, Grimstad, Norway. His research interests include cyber-physical systems, autonomous systems, and wireless embedded systems.

● ● ●